University of Glasgow
DEPARTMENT OF
AEROSPACE
ENGINEERING

Prediction of Unsteady Flow Around Square and Rectangular Section Cylinders Using a Discrete Vortex Method.

I. J. Taylor and M. Vezza

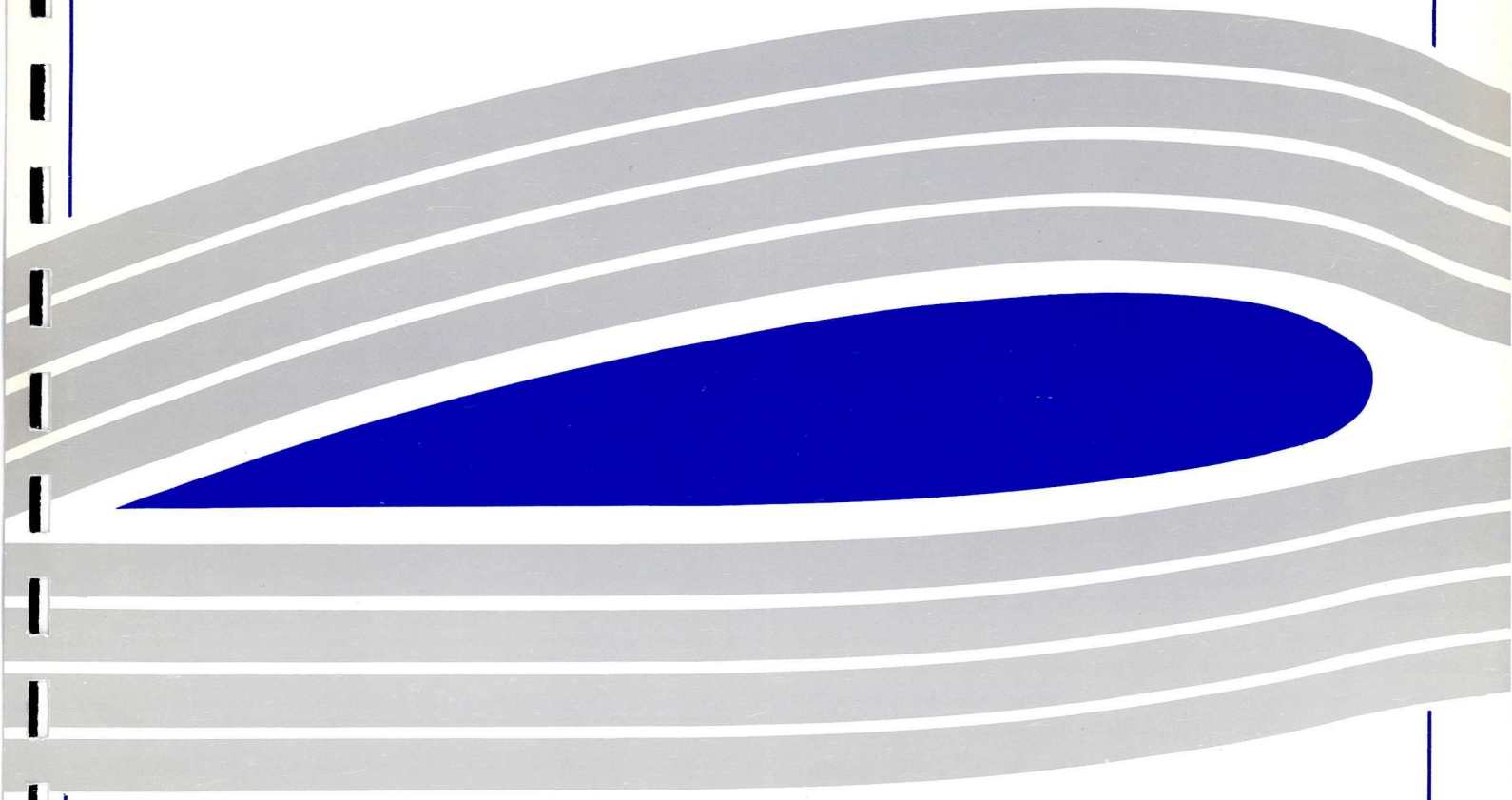

G.U. Aero Report No. 9801

Prediction of Unsteady Flow Around Square and Rectangular Section Cylinders Using a Discrete Vortex Method.

I. J. Taylor and M. Vezza

Department of Aerospace Engineering
James Watt Building South
University of Glasgow
Glasgow G12 8QQ

January 1998

Prediction of Unsteady Flow Around Square and Rectangular Section Cylinders using a Discrete Vortex Method.

Ian Taylor[1] and Marco Vezza[2]

Department of Aerospace Engineering, University of Glasgow, Glasgow, G12 8QQ, Scotland, UK.

ABSTRACT :

A Discrete Vortex Method has been developed at the Department of Aerospace Engineering, University of Glasgow to predict unsteady, incompressible, separated flows around closed bodies. The basis of the method is the discretisation of the vorticity field, rather than the velocity field, into a series of vortex particles which are free to move in the flow. The grid free nature of the method allows analysis of a wide range of problems for both stationary and moving bodies. This report presents a brief description of the numerical implementation, and presents the results of an extensive validation of the method on bluff body flow fields. Results are presented for the mean force coefficients, surface pressure coefficients and Strouhal numbers on a square section cylinder at varying angle of incidence. Also presented are the mean force coefficients and Strouhal numbers on rectangular cylinders. The results from the vortex method show good agreement, both qualitative and quantitative, with results taken from various experimental data.

1. Introduction.

The knowledge of the flow field around bluff structures is of major importance in the fields of civil and wind engineering. As modern structures become ever taller or longer, the structural response to aerodynamic forcing, due to phenomena such as vortex shedding, has a greater impact on the design of these structures. Accurate prediction of the flow field for such problems using computational methods is becoming increasingly important. Although this presents a challenge to computational methods, recent developments in both software and hardware make the use of these methods ever more valuable to the civil engineer.

---

[1] Postgraduate Researcher : Department of Aerospace Engineering.
[2] Lecturer : Department of Aerospace Engineering.

Discrete vortex methods have undergone significant development in recent years and have proven to be particularly well suited to the analysis of incompressible, unsteady and highly separated flow fields. Comprehensive reviews of vortex methods are given in [1-3]. The method is based on the discretisation of the vorticity field, rather than the velocity field, into a series of vortex particles. Each of these particles is of finite core size, and carries a certain amount of circulation. Particles are tracked in the flow field that they collectively induce. The Lagrangian nature of the method significantly reduces some of the problems associated with more traditional grid based methods, such as numerical diffusion and difficulties in achieving good resolution of small scale vortical structures. The concentration of vortex particles in areas of non-zero vorticity enables vortex methods to capture these small scale structures in more detail.

This paper presents a two dimensional discrete vortex method (DVM) that has been developed at the Department of Aerospace Engineering, University of Glasgow. The model was originally developed to analyse the dynamic stall phenomena on aerofoils undergoing a pitching motion [4-6]. The DVM presented herein employs a novel surface shedding model, involving partial release of the nascent vortex particles into the wake, which has been a major factor in solution quality to date.

The DVM has now successfully been generalised to model the flows around bluff bodies. The results of the validation of the method on both square and rectangular section cylinders are presented in this paper, as are comparisons with experimental data and results from other computational methods. The results demonstrate the capability of the method to accurately predict the variation of the flow field around a square section cylinder at a range of angles of incidence. Also, the general nature of the DVM is demonstrated, with the successful prediction of the mean force coefficients and Strouhal numbers for rectangular cylinders at different aspect ratios.

Validation of the DVM is now continuing on more complex test cases, including the analysis of oscillating bodies. The encouraging results obtained to date on the static cases, highlight the potential of the method to analyse moving body problems. The grid free nature of the method makes it well suited to analysis of these oscillatory cases. The successful validation for stationary bodies and early results for moving bodies, show that the DVM developed at the University of Glasgow is becoming a powerful tool for determining the sectional aerodynamic and aeroelastic characteristics of bodies typical of those found in many wind engineering applications.

2.0 Discrete Vortex Method.

2.1 Governing Equations.

Two-dimensional incompressible flow is governed by the following continuity and full viscous Navier-Stokes equations :

$$\nabla.\mathbf{U} = 0 \tag{1}$$

$$\frac{D\mathbf{U}}{Dt} = -\frac{1}{\rho}\nabla P + \nu\nabla^2\mathbf{U} \tag{2}$$

where $\mathbf{U}$ is the flow velocity, ρ is the fluid density, P is the pressure and ν is the kinematic viscosity. The solutions are subjected to the boundary conditions

$$\mathbf{U} = \mathbf{U}_i \text{ on } S_i \text{ and } \mathbf{U} = \mathbf{U}_\infty \text{ on } S_\infty \tag{3}$$

where i is the index for the body (Fig. 1). The boundary condition indicates that the flow in the far field is undisturbed and that the velocity of each vortex particle is equal to that of the body at the surface due to the no slip and no penetration conditions.

Using the definition of vorticity, $\vec{\omega} = \nabla \times \vec{\mathbf{U}}$ with $\vec{\omega} = \vec{\mathbf{k}}\omega$, and defining a vector potential, $\vec{\Psi}$ such that, $\vec{\mathbf{U}} = \nabla \times \vec{\Psi}$, $\vec{\Psi} = \vec{\mathbf{k}}\Psi$, $\nabla.\vec{\Psi} = 0$, then the governing equations (1) and (2) can be rewritten in vorticity/stream function form :

$$\nabla^2\Psi = -\omega \tag{4}$$

$$\frac{D\omega}{Dt} = \nu\nabla^2\omega \tag{5}$$

with the boundary condition given by

$$\nabla\Psi = \nabla\Psi_i \text{ on } S_i \text{ and } \nabla\Psi = \nabla\Psi_\infty \text{ on } S_\infty \tag{6}$$

The velocity field within the area of the body, depicted in Figs. 1 and 2, corresponds to that of a solid region with reference point c

$$\mathbf{U}_i = \mathbf{U}_{ic} + \Omega_i \times (\mathbf{r} - \mathbf{r}_{ic}) \tag{7}$$

where $\mathbf{U}_{ic}$ is the velocity of the reference point and Ω_i is the rotational velocity of the body. This is represented in stream function form by

$$\nabla^2 \Psi_i = -2\Omega_i \tag{8}$$

The relationship between the velocity and the vorticity has been derived by the application of Green's Theorem to (4) for region F (Fig. 1) and (8) for region B_i, and combining them through the boundary conditions [7]. For a point p outside the solid region, the velocity is given by :

$$\begin{aligned} \mathbf{U}_p = \mathbf{U}_\infty &+ \frac{1}{2\pi}\int_{F_b} \omega \frac{\mathbf{k}\times(\mathbf{r}_p - \mathbf{r})}{\|\mathbf{r}_p - \mathbf{r}\|^2} \mathrm{d}F_b \\ &+ \frac{1}{2\pi}\int_{F_w} \omega \frac{\mathbf{k}\times(\mathbf{r}_p - \mathbf{r})}{\|\mathbf{r}_p - \mathbf{r}\|^2} \mathrm{d}F_w + \frac{1}{2\pi}\int_{B_i} 2\Omega_i \frac{\mathbf{k}\times(\mathbf{r}_p - \mathbf{r})}{\|\mathbf{r}_p - \mathbf{r}\|^2} \mathrm{d}B_i \end{aligned} \tag{9}$$

where $F=F_b \cup F_w$ and $F_b \cap F_w = 0$. Equation (9) details the four contributions to the velocity from the freestream , the vorticity in the small control area around the solid region, the vorticity in the remaining flow area and the vorticity inside the solid region due to the motion of the body.

2.2 Numerical Implementation.

The numerical implementation of the governing equations is presented in more detail in Lin et al [4,5 and 7] and only a brief summary is presented below. For a two dimensional body, a polygonal representation of the body surface is created connecting a series of N node points that define the surface with straight lines to form a series of panels. Each panel is further subdivided into K equal length sub-panels. The thin area near the body surface is regarded as a special zone, the control zone, in which the vorticity is created. The vorticity in the remainder of the flow field arises through convection and diffusion of the vorticity generated in the control zone.

The vorticity in the control zone can be treated as a one dimensional vortex sheet, which is then discretised using a two stage process. First, the vorticity in the control zone, γ, is treated as a quantity that varies piecewise linearly and continuously along the surface. The values of γ at the node points therefore represent the entire vorticity distribution within the control zone. Secondly, the panel distribution of vorticity is further broken down into vortex blobs, one for each sub-panel. The blob is positioned a distance δ above the middle of the sub-panel. This process is illustrated in Fig. 3.

The γ values in the creation zone are the solution of the equations from the boundary condition which is implemented by ensuring zero mass flow through each surface panel. The implementation is expressed as

$$F_{js} + F_{ji} + F_{jf} + F_{jv} + F_{jn} = 0 \tag{10}$$

where each term represents the contribution of the mass flow from different sources. The first and second terms are from the motion of the body, with the remaining terms representing the contributions from the freestream, the vortices in the wake and the vortices within the control zone. The total number of equations (10) is N for a body with N panels, but only N-1 are independent as there is no source or sink within the body. Hence when N-1 panels satisfy zero mass flow, the mass flow for the final panel will automatically be zero. A further equation required to make the solution unique is obtained from Kelvin's theorem. The circulation of the vortices in the entire flowfield remains constant because there is no external source of vorticity. For each body, the additional condition is

$$\sum_{v} \Gamma_v + \sum_{j=1}^{N} \sum_{m=1}^{K} (\Gamma_j)_m + 2\Omega_i A_i = \Gamma_{st} \tag{11}$$

where the first term is the circulation of the vortices in the wake, the second is the circulation of the vortices in the control zone, the third is the circulation due to the body rotation and the fourth is the initial circulation in the flow field prior to the start of the calculation. The second term contains the unknown γ values. The strengths of the nascent vortices in the control zone are obtained once the equations are solved for the N γ values.

All vortices outside the control zone originate from nascent vortices. Their positions are the result of convection and diffusion at each time step. The simulation of vortex convection and diffusion employs an operator splitting technique, where the vorticity transport equation (5) is split into a separate convection part (12) and diffusion part (13), both of which are solved sequentially as proposed by Chorin [8].

$$\frac{D\omega}{Dt} = 0 \tag{12}$$

$$\frac{\partial \omega}{\partial t} = \nu \nabla^2 \omega \tag{13}$$

The convection velocity is equal to that of the associated particle and can be evaluated by equation (9). The diffusion process is modelled using a random walk procedure [8] which satisfies the Gaussian distribution of zero mean and standard deviation $\sqrt{2\Delta t / Re}$, where Δt is the timestep and Re is the Reynolds number of the flow. The exchange of vorticity between the control zone and the wake, or the release and absorption of vortex particles from/to the wake are

determined by the new vortex positions at the next instant of time, with respect to the surface position.

As the wake develops downstream of the body, three dimensional effects play a major role in the stretching of vortex filaments, and effectively redistribute vorticity in each direction. The effect of this is to reduce the strength of the von Karman vortices forming the vortex street. Various researchers have demonstrated this experimentally, showing, in particular, the transfer of spanwise vorticity ω_z to streamwise vorticity ω_x [9-11]. To account for this process in the DVM, a decay of the circulation in the wake downstream of the body is employed. This decay is similar in nature to that used by Basuki and Graham [12] and is given by

$$\Gamma(t) = \Gamma(0)\left[1 - \exp(-\tfrac{c}{t-t_c})\right] \tag{14}$$

where $\Gamma(t)$ is the circulation of the vortex particle, $\Gamma(0)$ is the initial circulation, t_c is the time of creation of the vortex and c is a decay constant. Lin et al [9] estimate from experimental results that, at a plane one diameter downstream of a circular cylinder, the circulation of the von Karman vortices has reduced by approximately 20% due to the transfer of vorticity from the spanwise component. The constant was chosen to produce a rate of transfer of circulation from the spanwise direction that is consistent with results from Lin. In order to conserve total circulation (11), the decayed vorticity is transferred to infinity. The inclusion of the vortex decay model allows the effects of three dimensionality in the body wake to be modelled in a relatively straightforward way.

The calculation of the velocity of a single vortex particle requires the influence of all regions of vorticity in the flow field to be taken into account (9). For a flow field containing N particles this leads to an operation count of $O(N^2)$, which becomes prohibitive as N increases. A fast algorithm for the velocity calculation has been included in the DVM and is presented in [13]. The procedure uses a zonal decomposition algorithm for the velocity summation. This allows the effect of groups of particles on the velocity to be calculated using a single series expansion, thus significantly reducing the operation count of the calculation. The algorithm utilises a hierarchical technique similar in nature to the adaptive Fast Multipole Method [14], so that the largest possible group of particles is used for each series expansion. The resulting operation count is O(N+NlogN), and therefore offers a significant improvement to the calculation efficiency. The calculations were performed on a Silicon Graphics Indigo workstation, typically using a 150MHz IP22 R4400 processor, with 16Kb cache size and 64Mb main memory size. A calculation around a square cylinder a 0° incidence for 7000 timesteps requires approximately 19-20hrs CPU.

3.0 Results and Discussion.

The flow fields around bluff bodies with square and rectangular cross sections for smooth onset flow, have been computed using the DVM. The effect of varying the angle of incidence from 0° to 45° is shown for the square section cylinder. Also, results are presented for rectangular section cylinders, with varying aspect ratios ranging from 0.25 to 3.0. Some typical results are presented, showing comparisons with experimental data and results from other computational methods. In each case, the across-wind body dimension, L, was used as the characteristic flow dimension (Fig. 2). All calculations were performed using an impulsively started flow field. The mean quantities presented below are calculated from the time-dependent data once the flow has settled into a fairly regular oscillatory pattern and the effects of the impulsive start become negligible.

3.1 Square Section Cylinder.

The calculations were performed at a Reynolds number of 20000, with a time step of 0.02 and with the nascent vortex particles being created $0.0025L$ from the surface. The body surface was represented by 160 equal length panels. The nascent vorticity was discretised using 7 vortices per panel to ensure overlapping of the vortex particles, and provide accurate resolution of the vorticity distribution on the body surface. The corners of the square are labelled as shown in Fig. 4.

3.1.1 General Flow Field Visualisation.

Figures 5 and 6 show the flow field around the square section cylinder at two different angles of incidence. In each case, the flow at various stages of the vortex shedding cycle are shown, using the distribution of particles from the DVM, accompanied by velocity vector plots to give more clarity to the predicted flow field. In general, the qualitative prediction of the flow fields are good. The alternate vortex shedding from the body, giving rise to a classical vortex street, can clearly be seen in the 0° case (Fig. 5). At 15° incidence, the shear layer separating from the front lower corner of the body, is clearly shown to be reattaching on the lower side face (Fig. 6). The effect that this reattachment has on the mean force coefficients will be discussed in more detail in the next section. The differences in the wake structure between the two cases can clearly be discerned, with noticeably weaker vortex shedding in the 15° case.

3.1.2 Mean Aerodynamic Force Coefficients : C_d and C_l.

Sample time histories for the lift and drag coefficients are shown in Fig. 7. The impulsive nature of the start to the calculation can clearly be seen. However, the flow settles down, in a relatively

short period of time, to the expected fairly regular oscillatory cycle, typical of bluff body flow fields.

The mean aerodynamic force coefficients, C_l and C_d at angles of incidence ranging from $\alpha = 0°$ to 45° are shown in Fig. 8 and 9 compared with experimental data. [15-21]. A summary of some of these results is compared in Table 1 with data from various other computational methods and experiment. The correct variation of both C_l and C_d with incidence is predicted, with good quantitative agreement with various experimental data being shown. The selected 2D CFD methods, in particular, do not capture the variation in the lift and drag, at the higher angle of incidence.

Authors	Angle (degrees)	Reynolds Number	Mean C_l	Mean C_d
DVM	0	2.0e+4	0.019	2.38
	15		-0.80	1.59
Lee [15] (exp.)	0	1.76e+5	0.021	2.04
	15		-0.72	1.58
Norberg [18] (exp.)	0	1.3e+4	0	2.15
	15		-0.68	1.80
Naudascher et al [17] (exp.)	0	1.06e+5	0	2.00
	15		-0.54	1.59
Blevins [22] (vortex method)	0	1.0e+4 - 1.0e+5	-	1.56
Koutmos et al [23] (2D CFD)	0	14285	-	2.37
Murakami et al [24] (2D CFD)	0	1.0e+5	0	2.09
Tamura et al [25] (2D CFD)	0	1.0e+4	0	2.4
	15		-1.2	2.3
Tamura et al [25] (3D CFD)	0	1.0e+4	0	2.2 - 2.3
	15		-0.84	1.74

Table 1 - Comparison of Mean Force Coefficients.

As the angle of incidence increases, the mean C_d reduces primarily due to the shear layer that is shed from corner D intermittently contacting corner C (Fig. 4). Eventually, when α is approximately 15°, this shear layer reattaches completely to form a separation bubble on face DC. The shear layer that originally separated from D, now separates from C, and hence gives rises to a narrower wake and a lower mean C_d. Further increases in α simply serve to increase the width of the wake, so giving rise to the gradual increase in C_d between 15 and 45°. The vortex method predicts this trend well, although the minimum C_d is predicted at 15° rather than the 12-

13° indicated in the experimental data. As shown above, the attached shear layer can clearly be seen at the higher incidence (Fig. 6).

The variation of C_l with incidence can also be explained by the reattachment of the shear layer to face DC. The separation bubble causes higher local suction pressures than those on face AB, and hence give rise to a negative lift coefficient, with a maximum at 15° when the shear layer is fully reattached. As the angle of incidence increases further, the separation bubble becomes smaller, so reducing the high local suction pressures on face DC, leading to a gradual increase in C_l. The results obtained from the vortex method again compare well with experimental data. A feature of the accuracy of the variation of the mean C_d and C_l with incidence demonstrate that the DVM could potentially be a useful tool for analysing galloping.

3.1.3 Mean Base Pressure Coefficient : C_{pb}.

The mean base pressure coefficient was calculated as the average of the pressure coefficient at the mid and quarter points on the leeward face of the body. This is consistent with many researchers, although some base pressure measurements are taken from the centre of the leeward face only. However, as the pressure in the base region on the square cylinder is reasonably constant, comparisons can be made with each set of data. The variation of mean base pressure with incidence is shown in Fig. 10. The results from the DVM show good qualitative and quantitative agreement with experimental data, though there is slightly too much suction at the lower angles of incidence, consistent with the slight over prediction of C_d at low incidence.

Previous researchers have shown that the base pressure is directly related to the amount of vorticity shed from each side of the body [15,26], which is in turn related to the distance required from the leeward face for vortex formation. Bearman and Trueman [26] showed that the greater the distance that the vortices are formed from the body, the less suction there will be in the base region. Hence, from the over prediction of the suction in the base region at low incidence, it can be deduced that the DVM predicts vortex formation somewhat closer to the body than occurs in practice (Fig. 5).

3.1.4 Mean Moment Coefficient : C_m.

The moment coefficient about the centre of the square against incidence is presented in Fig. 11, compared with experimental data [18,27]. As shown in Fig. 2, a positive moment is taken to act in the clockwise direction. Good agreement is shown with the correct trend of C_m being shown with incidence. The minimum predicted moment occurs between 20-25°, which is a little higher

than shown in the experiment. However, the accuracy of the results suggest that the vortex method may be a useful tool for analysing torsional oscillation of structures.

3.1.5 Strouhal Number.

Spectral analysis was performed on the lift coefficient time history, to obtain the Strouhal number, St :

$$St = nL / \mathrm{U} \tag{15}$$

where n is the frequency of the vortex shedding, U is the freestream velocity, and L is the side length of the cylinder (Fig. 2).

Due to the impulsive start to the calculation, the analysis was performed on a number of complete oscillation cycles of the lift history, after the flow had stabilised. A spectral analysis was also performed on the pressure coefficient time history at the centre of the upper side face. In addition, the location of the stagnation point on the windward face was also analysed. The value of *St* obtained from each of these methods was found to be consistent, and only the results from spectral analysis of the lift coefficient time history are presented below.

Authors	Angle (degrees)	Reynolds Number	St
DVM	0	2.0e+4	0.1278
	15		0.1467
Lee [15] (exp.)	0	1.76e+5	0.1214
	15		0.1424
Norberg [18] (exp.)	0	1.3e+4	0.1322
	15		0.1466
Obasaju [21] (exp.)	0	4.74e+4	0.1269
	15		0.1427
Koutmos et al [23] (2D CFD)	0	14285	0.178 [3]
Murakami et al [24] (2D CFD)	0	1.0e+5	0.132
Tamura et al [25] (2D CFD)	0	1.0e+4	0.103
	15		0.129
Tamura et al [25] (3D CFD)	0	1.0e+4	0.13
	15		0.18

Table 2 - Strouhal Number from Various Authors.

[3] Calculation in channel, with high blockage of 19%. Results appear to be uncorrected for blockage.

The variation of *St* with incidence is shown in Fig. 12, along with selected experimental data. Also, a summary of some of the results is compared with data from various other computational methods and experiments in Table 2. The DVM results compare well with data from other researchers. The 3D CFD results of Tamura and Kuwahara [25] fail to accurately predict the correct variation of *St* at incidence, although this code did give good results for the mean lift and drag coefficients (Table 1).

The correct trends are predicted with a gradual increase in *St* until a peak is reached at approximately 20°. This is a little higher than experimental values, although a wide range of results has been presented by various researchers. The DVM overpredicts to some degree the vortex shedding frequency at the higher angles of incidence. However, the strength of the vortex shedding and the resulting oscillation in the lift distribution is much weaker at the higher angles of incidence, hence giving rise to a wide range of values for *St*.

An interesting feature to note between 0° and 12° incidence, is that some researchers show a steady increase in *St* from 0° incidence, whereas others show a decrease in *St* before increasing to the peak value at approximately 13°. The reason for this behaviour is unclear, however in general terms a decrease in the width of the wake can be linked to an increase in *St*. The reattachment of the shear layer to the lower side face is the angle at which the wake is narrowest, and corresponds to the maximum *St* at 13°. In the cases where *St* initially decreases, the increase in the cross body dimension probably has most effect on the wake width, causing a wider wake. Whereas the gradual increase in *St* is probably more dependant on the intermittent reattachment of the shear layer at corner C (Fig. 4). The wide range of results demonstrate the sensitivity of *St* to the flow field, and emphasise the good quantitative agreement between the DVM and experiment.

3.1.6 Pressure Coefficient on Body Surface.

The pressure coefficient around the body for the 0° case is shown compared with experimental data [15,19,29 and 30], and with other computations [24] in Fig. 13. The results are plotted against distance along the body surface, from the centre of the windward face and moving clockwise around the body, as shown in Fig. 4. The pressure coefficient is normalised using the pressure at the stagnation point as the reference pressure. The pressure coefficient at 10° incidence is shown in Fig. 14.

In general, good agreement is shown with experimental data, although the high suction on the leeward face is a symptom of the slightly high prediction of C_d at 0°. The results also appear more favourable compared with those derived from both 2D and 3D CFD calculations [24]. The

discrepancy in the 2D results can be attributed to the lack of modelling of the 3D effects in the wake, such as the development of streamwise component of vorticity, ω_x, due to the vortex stretching and roll up of the spanwise von Karman vortices as discussed in section 2. The vortex decay calculation was included in the DVM to account for these 3D effects.

The results from the vortex method compare well with those calculated from full 3D methods, which use $O(10^5)$ grid points. From the high base pressure on the leeward face of the 3D CFD calculation, the resulting mean drag coefficient is likely to be lower than experiment. It is likely that such a detailed analysis using a full 3D model would require significantly higher computational effort than a 2D vortex model. [4]

The predicted mean pressure coefficient at 10° incidence also compares well with experimental data. The results demonstrate that the effects of higher angles of incidence on the pressure distribution are successfully predicted by the DVM. Notably, the displacement of the stagnation point along the windward face, and the effects of the reattaching shear layer at corner C have been captured.

3.1.7 RMS Fluctuating Pressure Coefficients.

The rms lift coefficient for the 0° case was calculated to be 1.369. This compares well with experimental data, with various researchers giving values ranging between, 1.20 and 1.35 [15, 28, 29 and 32].

The rms pressure fluctuations around the body surface are shown in Fig. 15 compared with various experimental data and with results from other computations. The vortex method results compare well with experiments, and on the side faces in particular, lies in the middle of a fairly wide range of results. The reduction of the fluctuations on the leeward face is also successfully predicted. The results from the 2D CFD calculation are quite poor, especially on the side face, whereas the 3D calculation shows generally good agreement with experiment. This can be attributed again to the 2D CFD method not taking account of the transfer of vorticity from the von Karman component due to 3D effects in the body wake. This is consistent with the results from the DVM, in that the predicted rms pressure fluctuations, particularly on the leeward face, were poor prior to the addition of the wake decay model.

[4] Conference presentation of [31] estimated that the calculation of one vortex shedding cycle, using 3D CFD method, with $O(10^6)$ grid points required approximately 20hrs CPU on a Cray supercomputer. This is compared to the DVM which typically requires 19-20hrs for a full calculation on an SG Indigo workstation (Section 2.1).

3.2 Rectangular Section Cylinders.

The DVM has also been validated for rectangular section cylinders at 0° incidence for aspect ratios ranging from 0.25 to 3.0. The calculations were again performed at a Reynolds number of 20000, with a time step of 0.02. As far as possible, the length of the surface panels were the same as in the square cylinder calculations to ensure consistency in the results. As mentioned above, the crosswind body dimension is used to non-dimensionalise the force coefficients and Strouhal numbers. The aspect ratio is defined as b/h where b is the length of the side parallel to the freestream velocity and h is the cross wind body dimension. As the calculations are presented for 0° incidence cases, only the variation of mean drag coefficients and Strouhal number are shown below.

3.2.1 Mean Drag Coefficient : C_d.

The variation of C_d with aspect ratio is shown compared with experimental data and other computations in Fig. 16. In general, good agreement is shown with the effect of aspect ratio on the results being well predicted by the DVM. The results also compare favourably with other computations. The most notable effect of aspect ratio on C_d is in the range b/h=0 to 1. A maximum value is reached at around b/h=0.62, the so called "critical section". At aspect ratios lower than the critical section, the vortex formation is relatively unaffected by the two leeward corners of the body. As the aspect ratio is increased towards the critical section, there is effectively a reduction between the base region and the vortex formation, resulting in an increased suction in the base region and hence a higher C_d [18 and 26]. Increasing the aspect ratio from the critical section, the influence of the leeward corners on the shear layers moves the vortex formation further downstream, leading to a reduction in the suction in the base region and hence a reduced C_d. The aspect ratio of the critical section is shown by the DVM to be between 0.6 and 0.7 and the C_d at this section is well predicted.

It is notable that the DVM gives a much better prediction of this trend than the vortex methods of both Blevins [22] and Bienkiewicz and Kutz [20]. In both of these cases, the peak C_d at the golden section is not predicted. Each of these two results show a gradual increase in C_d as the aspect ratio reduces.

3.2.2 Strouhal Number : *St*

The variation of Strouhal number with aspect ratio is shown in Fig. 17, compared with experimental data and other computations. The results from the DVM show good agreement with the data and compare well with the other computations. The Strouhal number behaves differently

to C_d at aspect ratios less than 1.0, with a gradual decrease in *St* as aspect ratio increases. The reason for this is that the dominant effect on *St* is the wake width.

At low aspect ratio, the width of the wake is generally constant as the shear layers separate from the front two corners of the body. Hence varying aspect ratio when *b/h* is less than 1.0 has little effect on *St*. Between aspect ratios of *b/h*=2.0 and 3.0, the shear layers separating from the windward corners reattach to the side faces of the body, resulting in a much narrower wake and a correspondingly higher vortex shedding frequency. Various experimental results show that this reattachment is intermittent, resulting in a "double" *St* for some aspect ratios between 2.0 and 3.0. The higher *St* corresponds to the case where the flow reattaches and the lower value is effectively a continuation of the decrease in *St* with aspect ratio.

This phenomena is well predicted by the DVM and is not demonstrated in the results of Bienkiewicz and Kutz [20], where the results are only given up to an aspect ratio of 2.0. The "double" Strouhal number is clearly seen in the experimental results of Norberg [18] and Ohtsuki et al [34].

4.0 Conclusions.

A Discrete Vortex Method (DVM) has successfully been developed at the Department of Aerospace Engineering, University of Glasgow. The method is based on the discretisation of the vorticity field, with vortex particles tracked in the flow field in a Lagrangian manner.

The DVM has been used to predict the flow field around static square and rectangular section cylinders. The results show good agreement with experimental data for mean force coefficients, Strouhal number and surface pressure coefficients. The variation of these quantities with angle of incidence for the square cylinder and aspect ratio for the rectangular cylinder, is demonstrated in the results of the DVM . The results also compare favourably with other computational methods.

Future research is aimed at extending the validation of the DVM to a wider range of geometries relevant to the field of wind engineering, such as suspension bridge deck sections. Also, the method is now being used to analyse moving body problems. The grid free nature of the method makes it well suited to analysis of these oscillatory cases. The results of this analysis will be published in a future report. The successful validation of the method for stationary bodies and the initial results for moving bodies show that the DVM is becoming a powerful tool for analysing the flow around bodies typical of those found in many wind engineering applications.

Acknowledgements.

The support and funding of this research by the Engineering and Physical Sciences Research Council (EPSRC) is gratefully acknowledged.

References.

1) SARPKAYA, T., 1989, "Computational Methods with Vortices - The 1988 Freeman Scholar Lecture." Journal of Fluids Engineering, Vol. 111, pp. 5-52.
2) LEONARD, A., 1980, "Vortex Methods for Flow Simulation." Journal of Computational Physics, Vol. 37, pp. 289-335.
3) PUCKETT, E.G., 1993, "Vortex Methods : An Introduction and Survey of Selected Research Topics." Incompressible Computational Fluid Dynamics, ed. M.D. Gunzb and R.A. Nicolaides, Cambridge University Press.
4) LIN, H. and VEZZA, M., 1996, "A Pure Vortex Method for Simulating Unsteady, Incompressible, Separated Flows around Static and Pitching Aerofoils." Proceedings of 20th ICAS Conference, Sorrento, Italy.
5) LIN, H., VEZZA, M. and GALBRAITH, R.A.McD., 1997, "Discrete Vortex Method for Simulating Unsteady Flow Around Pitching Aerofoils." AIAA Journal, Vol. 35, No. 3, pp. 494-499.
6) VEZZA, M., 1992, "A New Vortex Method for Modelling Two-Dimensional, Unsteady Incompressible, Viscous Flows." Dept. of Aerospace Engineering, University of Glasgow, G.U. Aero Report No. 9245, Glasgow, Scotland, UK.
7) LIN, H and VEZZA M, 1994 "Implementation of a Vortex Method for the Prediction of Separated Incompressible Flows." Dept. of Aerospace Engineering, University of Glasgow, G.U. Aero Report No. 9425, Glasgow, Scotland, UK.
8) CHORIN, A.J., 1973, "Numerical Study of Slightly Viscous Flow." Journal of Fluid Mechanics, Vol. 57, pp. 785-796.
9) LIN, J-C., VOROBIEFF, P. and ROCKWELL, D., 1995 "Three-Dimensional Patterns of Streamwise Vorticity in the Turbulent Near-Wake of a Cylinder." Journal of Fluids and Structures, Vol. 9, pp. 231-234.
10) STANSBY, P.K., 1985, "A Generalised Discrete-Vortex Method for Sharp-Edged Cylinders." AIAA Journal, Vol. 23, No. 6, pp. 856-861.
11) SARPKAYA, T. and SCHOAFF, R.L., 1979, "Inviscid Model of Two-Dimensional Vortex Shedding by a Circular Cylinder." AIAA Journal, Vol. 17, No. 11, pp. 1193-1200.
12) BASUKI, J. and GRAHAM, J.M.R., 1987, "Discrete Vortex Computation of Separated Airfoil Flow." AIAA Journal, Vol. 25, No. 11, pp. 1409-1410.

13) TAYLOR, I.J. and VEZZA, M., 1997, "Application of a Zonal Decomposition Algorithm, to Improve the Computational Operation Count of the Discrete Vortex Method Calculation." Dept. of Aerospace Engineering, University of Glasgow, G.U. Aero Report No. 9711, Glasgow, Scotland, UK.

14) CARRIER, J., GREENGARD, L. and ROKHLIN, V., 1988, "A Fast Adaptive Multipole Algorithm for Particle Simulations." SIAM Journal of Scientific and Statistical Computing, Vol. 9, pp. 669-686.

15) LEE, B.E., 1975, "The Effect of Turbulence on the Surface Pressure Field of a Square Prism." Journal of Fluid Mechanics, Vol. 69, Part 2, pp. 263-282.

16) ESDU, 1971, "Fluid Forces, Pressures and Moments on Rectangular Blocks." Engineering Sciences Data Item Number 71016.

17) NAUDASCHER, E., WESKE, J.R. and FEY, B., 1981, "Exploratory Study on Damping of Galloping Vibrations." Journal of Wind Engineering and Industrial Aerodynamics, Vol. 8, pp. 211-222.

18) NORBERG, C., 1993, "Flow Around Rectangular Cylinders : Pressure Forces and Wake Frequencies." Journal of Wind Engineering and Industrial Aerodynamics, Vol. 49, No. 1-3, pp. 187-196.

19) IGARASHI, T., 1984, "Characteristics of the Flow Around a Square Prism." Bulletin of the JSME, Vol. 27, No. 231, pp. 1858-1865.

20) BIENKIEWICZ, B. and KUTZ, R.F., 1993, "Aerodynamic Loading and Flow Past Bluff Bodies using Discrete Vortex Method." Journal of Wind Engineering and Industrial Aerodynamics, Vol. 46-47, pp. 619-628.

21) OBASAJU, E.D., 1983, "An Investigation of the Effects of Incidence on the Flow Around a Square Section Cylinder." Aeronautical Quarterly, Vol. 34, pp. 243-259.

22) BLEVINS, R.D., 1989, "Application of the Discrete Vortex Method to Fluid-Structure Interaction." Proceedings of Flow Induced Vibration, 1989 ASME Pressure Vessels and Piping Conference, Honolulu, HI, USA, 23-27 July, 1989, pub. ASME, Pressure Vessels and Piping Division. Vol. 154, pp. 131-140.

23) KOUTMOS, P. and MAVRIDIS, C., 1997, "A Computational Investigation of Unsteady Separated Flows." International Journal of Heat and Fluid Flow, Vol. 18, No. 3, pp. 297-306.

24) MURAKAMI, S. and MOCHIDA, A., 1995, "On Turbulent Vortex Shedding Flow past 2D Square Cylinder Predicted by CFD." Journal of Wind Engineering and Industrial Aerodynamics, Vol. 54-55, pp. 191-211.

25) TAMURA, T. and KUWAHARA, K., 1990, "Numerical Study of Aerodynamic Behaviour of a Square Cylinder." Journal of Wind Engineering and Industrial Aerodynamics, Vol. 33, No. 1-2, pp. 161-170.

26) BEARMAN, P.W. and TRUEMAN, D.M., 1972, "An Investigation of the Flow Around Rectangular Cylinders." Aeronautical Quarterly, Vol. 23, pp. 229-237.

27) NAKAMURA, Y. and MIZOTA, T., 1975, "Torsional Flutter of Rectangular Prisms." Journal of the Engineering Mechanics Division, ASCE, Vol. 101, pp. 125-142.

28) VICKERY, B.J., 1966, "Fluctuating Lift and Drag on a Long Cylinder of Square Cross-Section in a Smooth and in a Turbulent Stream." Journal of Fluid Mechanics, Vol. 25, Part 3, pp. 481-494.

29) BEARMAN, P.W. and OBASAJU, E.D., 1982, "An Experimental Study of Pressure Fluctuations on Fixed and Oscillating Square-Section Cylinders." Journal of Fluid Mechanics, Vol. 119, pp. 297-321.

30) HASAN, M.A.Z., 1989, "The Near Wake Structure of a Square Cylinder." International Journal of Heat and Fluid Flow, Vol. 10. No. 4, pp. 339-348.

31) TAMURA, T., MIYAGI, T. and KITAGISHI, T., 1997, "Numerical Prediction of Unsteady Pressures on a Square Cylinder with Various Corner Shapes." Proceedings of 2nd European and African Conference on Wind Engineering, Genova, Italy, 22-26 June 1997, pp. 815-822.

32) WILKINSON, R.H., 1981, "Fluctuating Pressures on an Oscillating Square Prism. Part 1 : Chordwise Distribution of Fluctuating Pressure." Aeronautical Quarterly, Vol. 32, No. 2, pp. 97-110.

33) COURCHESNE, J. and LANEVILLE, A., 1979, "A Comparison of Correction Methods Used in the Evaluation of Drag Coefficient Measurements for Two-Dimensional Rectangular Cylinders." Journal of Fluids Engineering, Vol. 101, pp. 506-510.

34) OTSUKI, Y., WASHIZU, K., TOMIZAWA, H. and OHYA, A., 1974, "A Note on the Aeroelastic Instability of a Prismatic Bar with Square Section." Journal of Sound and Vibration, Vol. 34, No. 2, pp. 233-248.

35) KNISELY, C.W., 1990, "Strouhal Numbers of Rectangular Cylinders at Incidence : A Review and New Data." Journal of Fluids and Structures, Vol. 4, pp. 371-393.

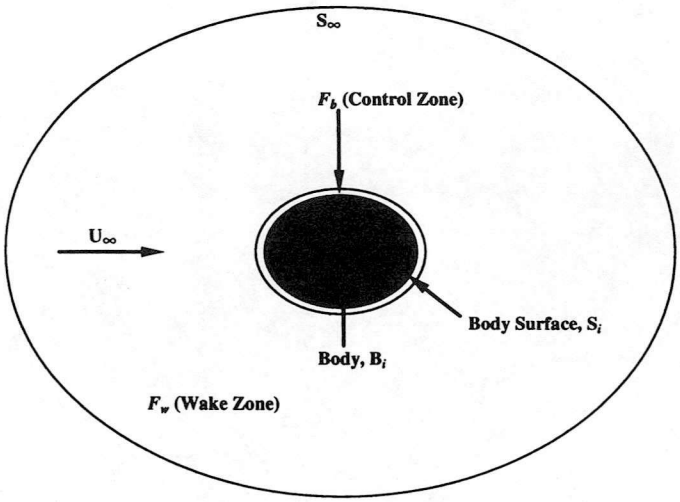

Fig. 1 - Flow Domain.

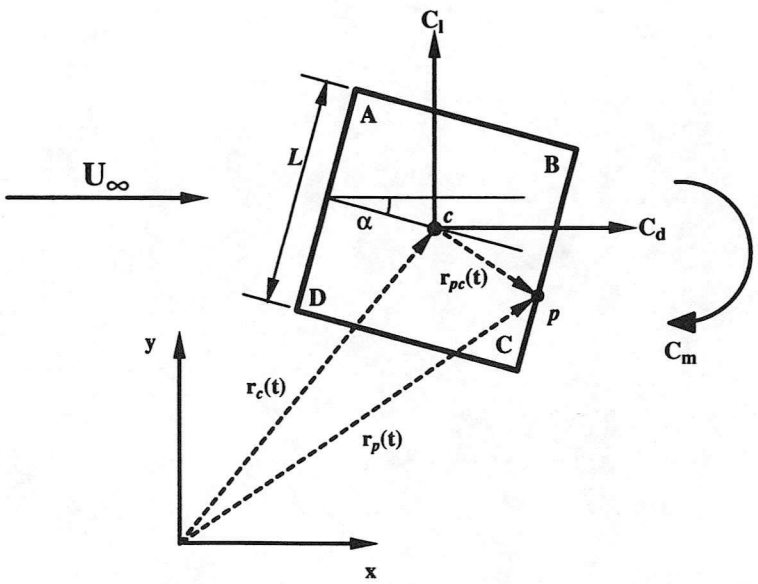

Fig. 2 - Body Orientation and Reference Coordinate System.

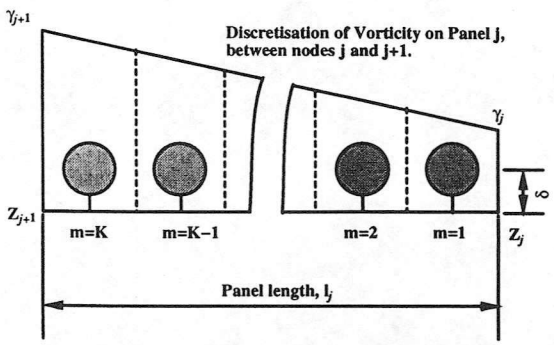

Fig. 3 - Discretisation of Vorticity and Subpanels.

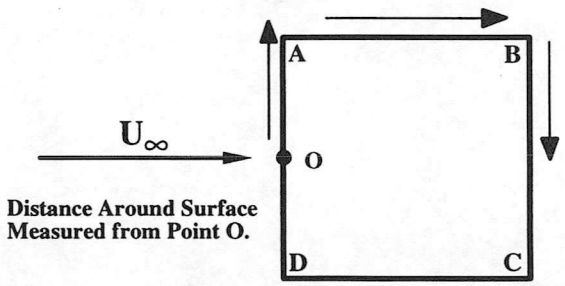

Fig. 4 - Labeling Conventions.

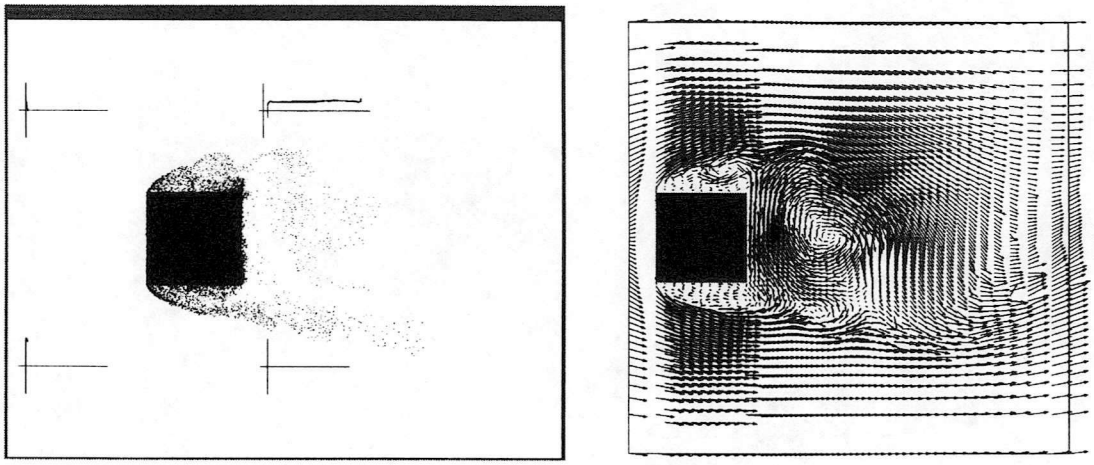

a) $t^* = 181.0$ ($t^* = tD/U$)

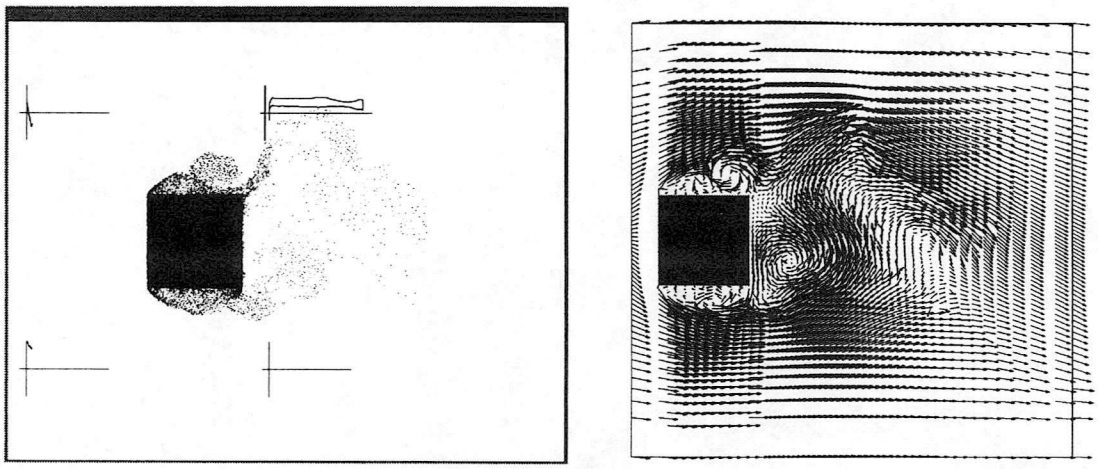

b) $t^* = 183.0$

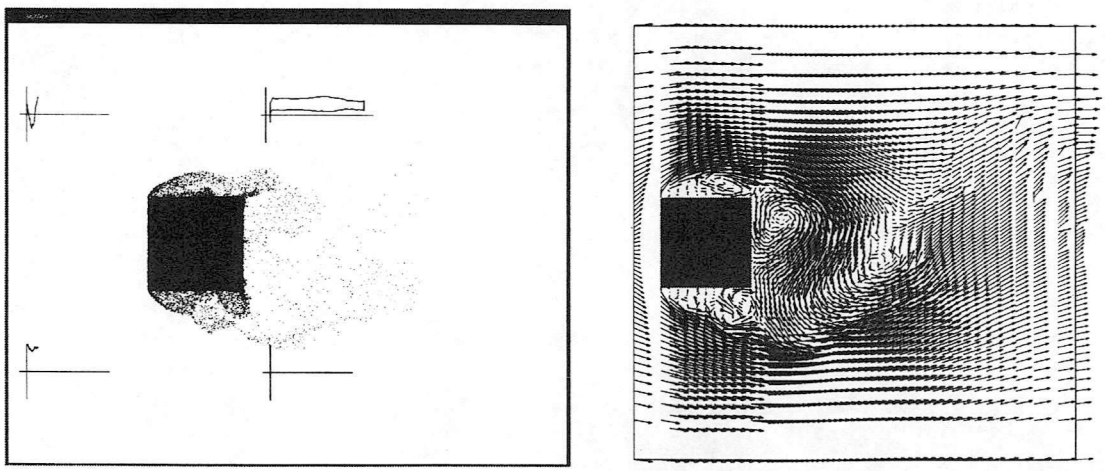

c) $t^* = 186.0$

Fig. 5 - Square Section Cylinder at 0 Degrees Incidence : Visualisation of Vortex Shedding.

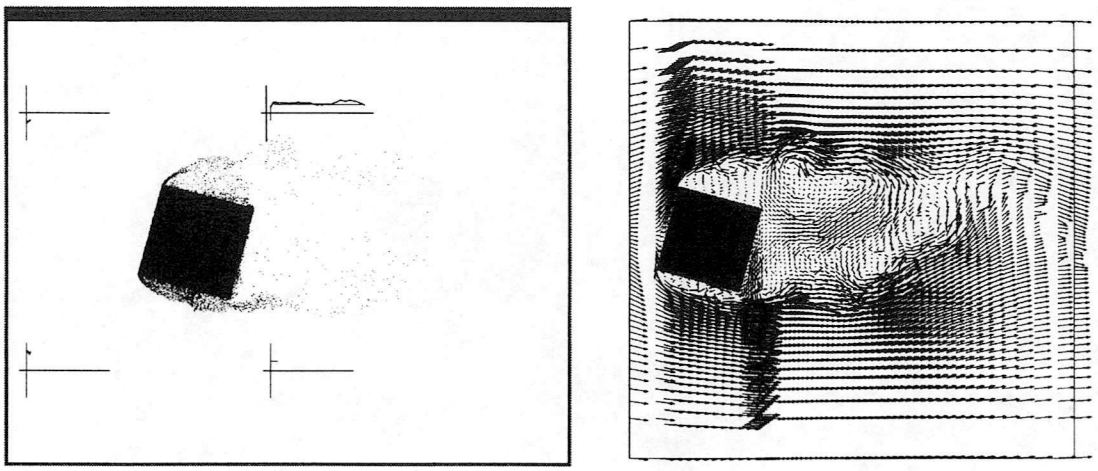

a) $t^* = 142.0$ $(t^* = tD/U)$

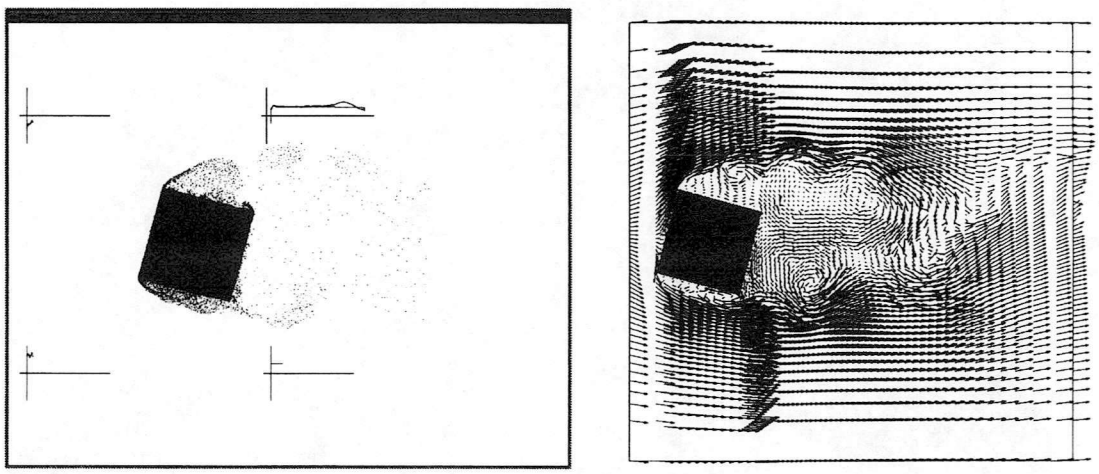

b) $t^* = 143.0$

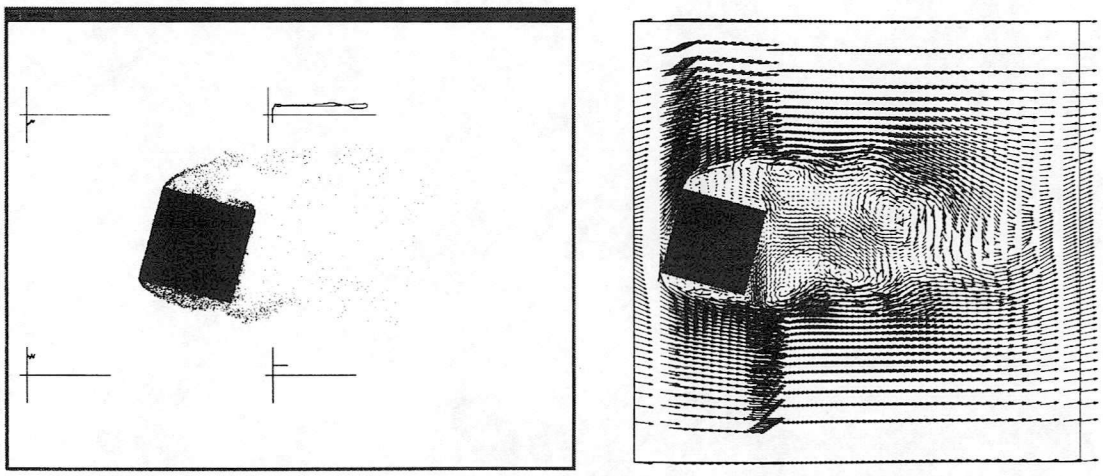

c) $t^* = 144.0$

Fig. 6 - Square Section Cylinder at 15 Degrees Incidence : Visualisation of Vortex Shedding.

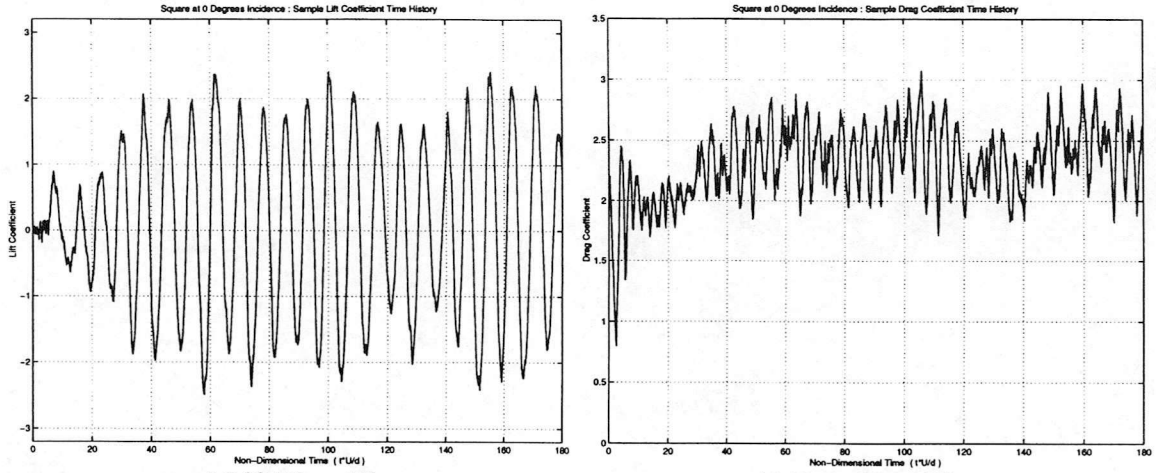

a) Lift Time History b) Drag Time History.

Fig. 7 - Square Cylinder :Sample Time History of Force Coefficients.

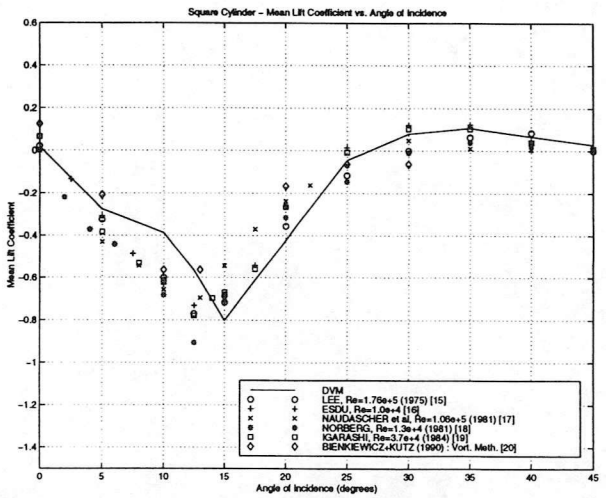

Fig. 8 - Square Cylinder : Mean Lift Coefficients vs. Angle of Incidence.

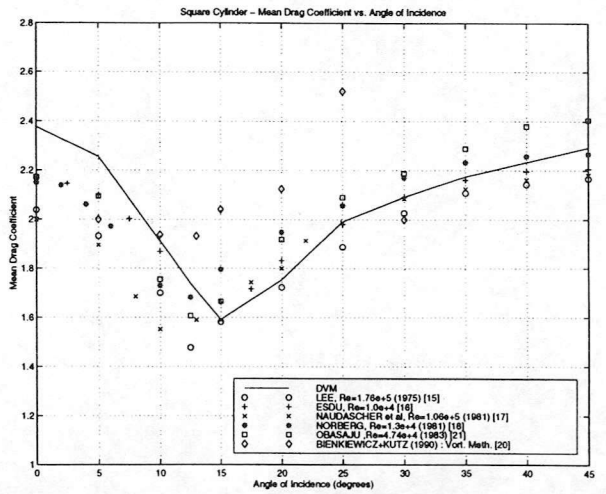

Fig. 9 - Square Cylinder : Mean Drag Coefficients vs. Angle of Incidence.

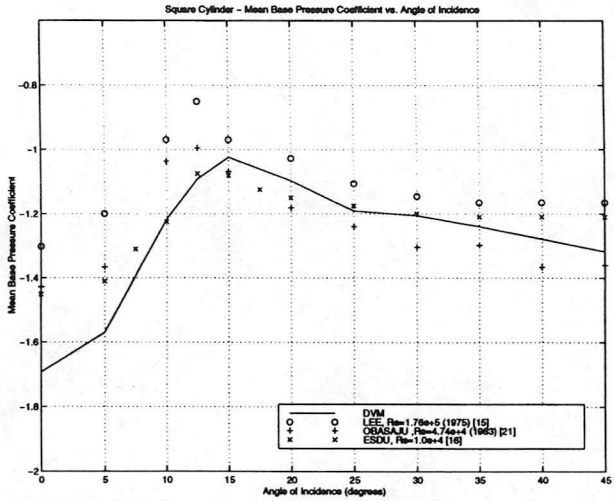

Fig. 10 - Square Cylinder : Mean Base Pressure Coefficient vs. Angle of Incidence.

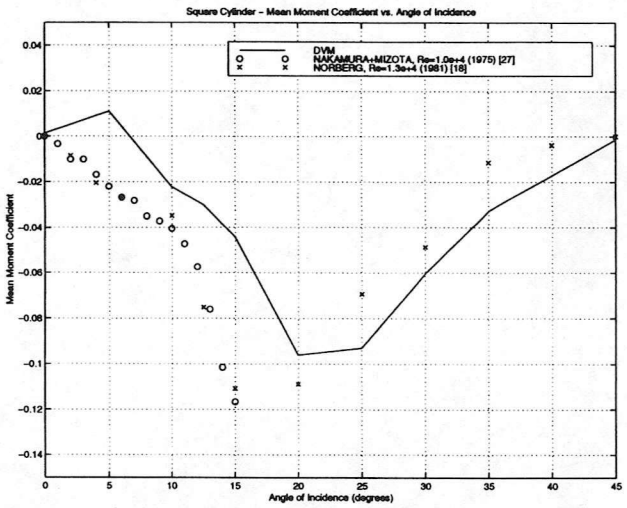

Fig. 11 - Square Cylinder : Mean Moment Coefficient vs. Angle of Incidence.

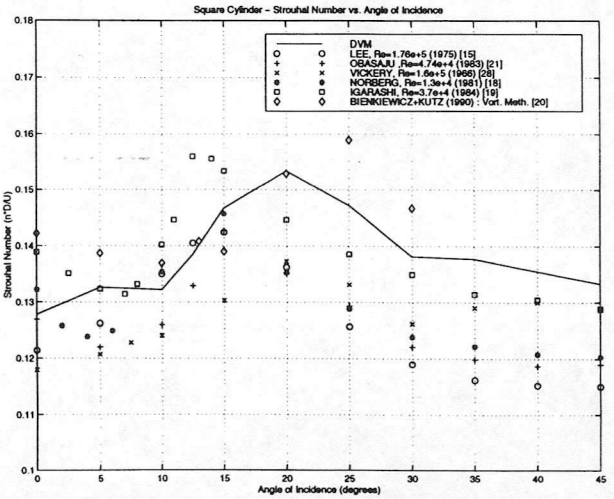

Fig. 12 - Square Cylinder - Strouhal Number vs. Angle of Incidence.

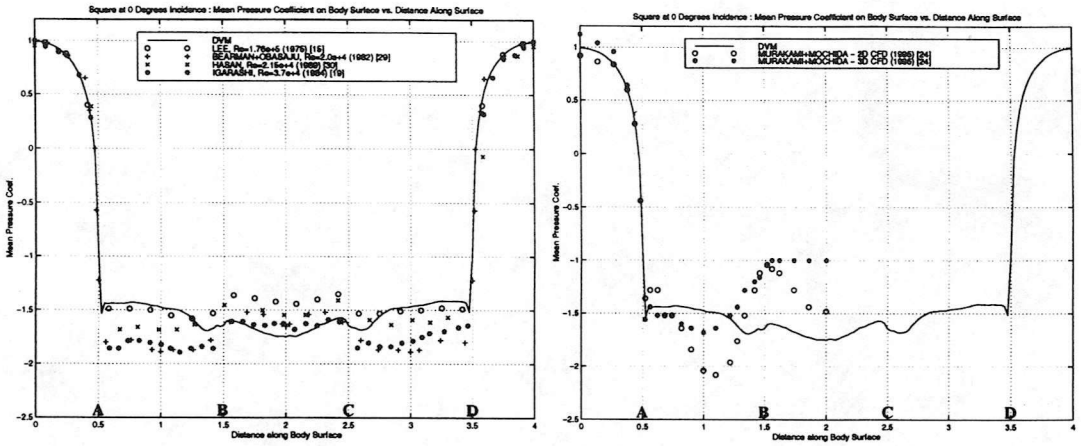

a) b)

Fig. 13 - Square Cylinder at 0° - Surface Pressure Coefficient vs. Distance Along Body Surface. (Note - The labels on the x-axis (A,B, etc.) refer the corners of the body as labelled in Fig. 4.)

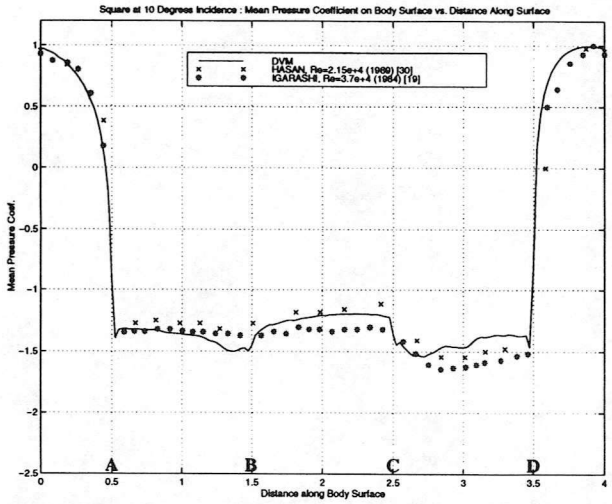

Fig. 14 - Square Cylinder at 10° - Surface Pressure Coefficient vs. Distance Along Body Surface.

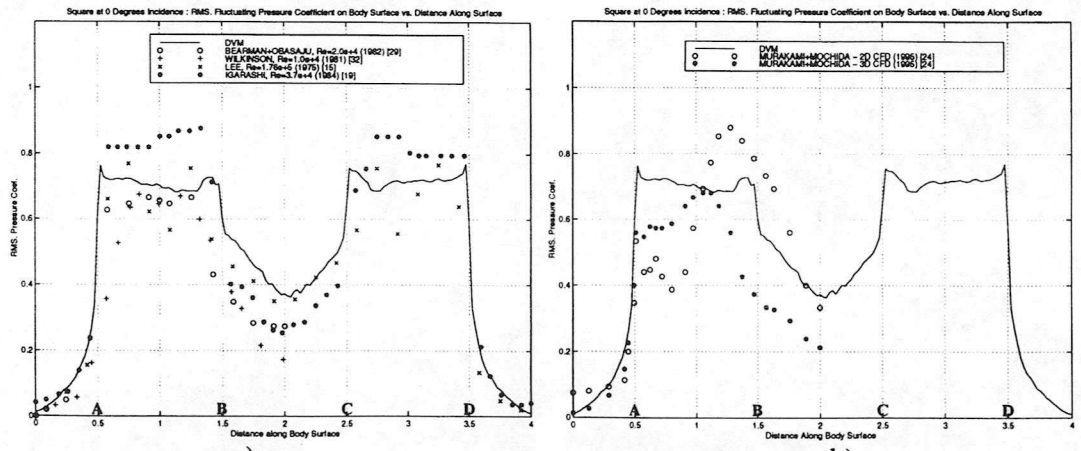

a) b)

Fig. 15 - Square Cylinder at 0° - RMS Pressure Fluctuations vs. Distance Along Body Surface.

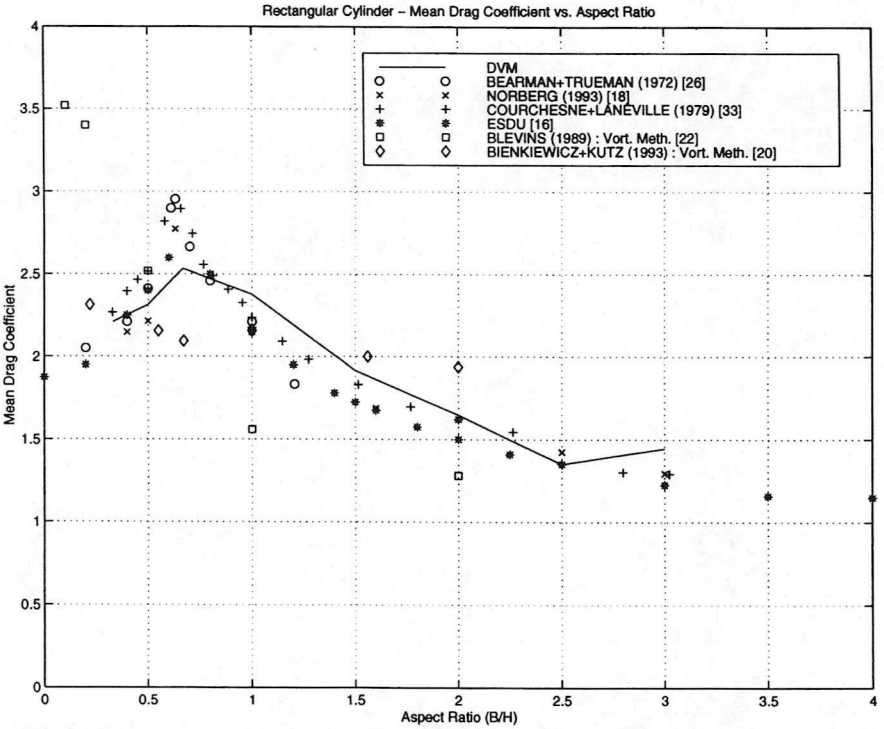

Fig. 16 - Rectangular Cylinders : Mean Drag Coefficient vs. Aspect Ratio (*b/h*)

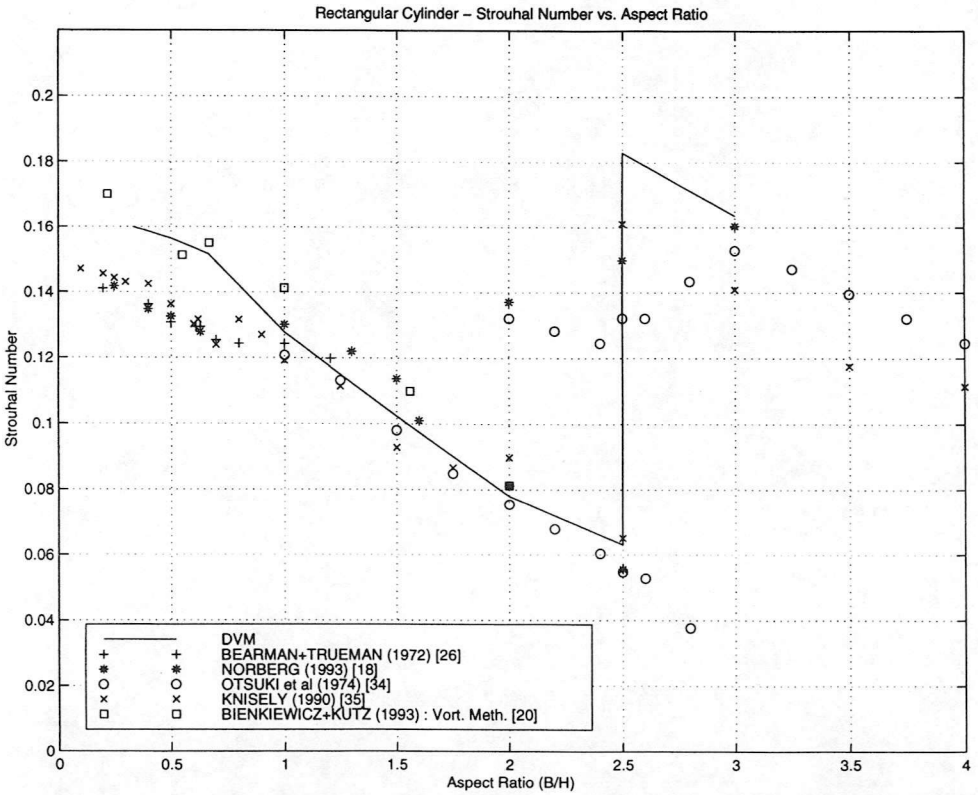

Fig. 17 - Rectangular Cylinders : Strouhal Number vs. Aspect Ratio (*b/h*)